Paper:
Lin, C., De Rossi, F., Kim, J., Baker, J., Ngiam, J., Xu, B., Pont, S., Aristidou, N., Haque, S., et. al. (2019). Evidence for surface defect passivation as the origin of the remarkable photostability of unencapsulated perovskite solar cells employing aminovaleric acid as a processing additive. *Journal of Materials Chemistry A, 7*(7), 3006-3011.
http://dx.doi.org/10.1039/C8TA11985F

Evidence for surface defect passivation as the origin of the remarkable photostability of unencapsulated perovskite solar cells employing aminovaleric acid as a processing additive

Chieh-Ting Lin[ab], Francesca De Rossi[c], Jinhyun Kim[a], Jenny Baker[c], Jonathan Ngiam[b], Bob Xu[b], Sebastian Pont[a], Nicholas Aristidou[a], Saif A. Haque[a], Trystan Watson[c], Martyn A McLachlan[*b], James R Durrant[*ac].

a. Department of Chemistry and Centre for Plastic Electronics, Imperial College London, Exhibition Road, London SW7 2AZ, U.K

b. Department of Materials and Centre for Plastic Electronics, Imperial College London, Exhibition Road, London SW7 2AZ, U.K.

c. SPECIFIC IKC, College of Engineering, Swansea University, Bay Campus, Fabian Way, Swansea SA1 8EN, U.K.

Corresponding author:

Martyn A McLachlan (martyn.mclachlan@imperial.ac.uk)

James R Durrant (j.durrant@imperial.ac.uk)

Abstract

This study addresses the cause of enhanced stability of methyl ammonium lead iodide when processed with aminovaleric acid additives (AVA-$MAPbI_3$) in screen printed, hole transport layer free perovskite solar cells with carbon top electrodes (c-PSC). Employing AVA as an additive in the active layer caused a 40-fold increase in device lifetime measured under full sun illumination in ambient air (RH ~15%). This stability improvement with AVA was also observed in optical photobleaching studies of planar films on glass, indicating this improvement is intrinsic to the perovskite film. Employing low-energy ion scattering spectroscopy, photoluminescence studies as a function of AVA and oxygen exposure, and a molecular probe for superoxide generation, we conclude that even though superoxide is generated in both AVA-$MAPbI_3$ and $MAPbI_3$ films, AVA located at grain boundaries is able to passivate surface defect sites, resulting in enhanced resistivity to oxygen induced degradation. These results are discussed in terms of their implications for the design of environmentally stable perovskite solar cells.

Main text

State of the art power conversion efficiencies (PCE) of laboratory scale organohalide lead perovskite solar cells (PSC) are now exceeding 22%, approaching PCEs achieved with silicon photovoltaics.[1,2] Interest in these solar cells is further motivated by their band gap tunability, high trap state tolerance, high absorption coefficients and potentially low fabrication costs.[3–6] However, attaining long term PSC device stability is still one of the key challenges for commercialization. This is particularly the case for devices exposed to environmental stress, with moisture, temperature, oxygen, light, and combinations of these, all being identified as potential causes of degradation.[7–9] Among these environmental stresses, the combination of oxygen and light has been shown to be a key degradation pathway for devices tested in ambient air under 1 Sun illumination.[7] This degradation pathway has been shown to be associated with the light driven reduction of oxygen to superoxide (O_2^-).[10] Several approaches, including for example introducing a superoxide scavenger, and tuning perovskite composition via cation/halide substitution, have been shown to be promising routes to enhance the stability of organohalide lead perovskite materials and devices under light and oxygen environmental stress.[11–13]

Among the range of thin film PSC architectures reported in the literature to date, the screen printed HTM free ('triple mesoscopic stack') architecture with carbon top electrode (c-PSC) is attracting particular interest due to its potentially low production costs, scalability and promising stability.[14] These devices comprise two layers of mesoporous inorganic metal oxide (TiO_2 and ZrO_2) and carbon top electrode, all infiltrated with perovskite light absorber methylammonium lead iodide ($MAPbI_3$) employing aminovaleric acid (AVA) iodide as a processing additive.[14] The fully printable device processing makes this architecture particularly attractive for scaling to large area fabrication.[15,16] Unencapsulated devices showed remarkable stability, exhibiting stable performance over 1000 hour under full sun illumination without encapsulation,[14] and over 1 year stability for encapsulated devices.[17] Although enhanced stability against moisture has been suggested to be related to either the ability of the zwitterionic AVA ligand to crosslink between the perovskite crystallites or to the tendency of AVA to drive the formation of 2D perovskite layers,[17–19] the origin of this promising stability and particularly the device's increased resistance to light and oxygen induced degradation, has not been determined to date.

In the study herein, we focus on the origin of the enhanced operational stability of unencapsulated c-PSC devices observed with the addition of AVA to the $MAPbI_3$ film (AVA-$MAPbI_3$). Unencapsulated c-PSC devices with AVA-$MAPbI_3$ are shown to exhibit ~ 40 times longer lifetimes than devices with $MAPbI_3$ under full sun illumination in ambient air. Remarkably, we find an analogous stability enhancement under similar stress conditions for planar thin films of neat AVA-$MAPbI_3$ versus $MAPbI_3$ deposited directly onto glass substrates, indicating this enhancement is not related to the $MAPbI_3$ / TiO_2 interface. Employing low-energy ion scattering spectroscopy and time-dependent photoluminescence, we conclude that, even though superoxide is generated in both AVA-$MAPbI_3$ and $MAPbI_3$ films, AVA located at grain surfaces is able to passivate defect sites, resulting in enhanced resistivity to oxygen induced degradation.

Multilayer screen printed mesoscopic stacks, comprising FTO/compact TiO_2/mesoporous TiO_2/mesoporous ZrO_2/mesoporous carbon, were fabricated using thermal annealing method as reported previously (Figure 1a).[14] These stacks were then infiltrated with $MAPbI_3$, or $MAPbI_3$ with 3% molar ratio of aminovaleric acid (AVA, Figure 1b), to complete the c-PSC devices. Initial power conversion efficiencies for $MAPbI_3$ devices averaged 10.8% (champion 11.1%) and AVA-$MAPbI_3$ devices averaged 8.7% (champion 9.1%), which are reasonable for fully printed devices (Figure S1a).[14,20] These device PCEs are mask-area dependent as we reported previously (Figure S1b and S1c) because of the poor conductivity of the carbon electrode limiting the fill factor.[21] $MAPbI_3$ and AVA-$MAPbI_3$ c-PSC devices were aged in ambient air (RH ~15%) under 1 sun illumination provided by LEDs without encapsulation. The devices were kept at open circuit voltage (Voc), and current-voltage scans undertaken every 30 minutes. As indicated in Figure 1c, the $MAPbI_3$ device rapidly lost 50% PCE within 2 hours, while the AVA-$MAPbI_3$ device required more than 86 hours for an equivalent efficiency loss. We note that aging devices at Voc can result in a more severe device degradation than at maximum power point or short circuit.[22] We previously reported that c-PSC with $MAPbI_3$ active layer showed outstanding ambient air (RH ~50%) shelf-lifetime (>3000 hours),[21] indicating that dark humidity exposure does not limit the lifetime of c-PSC studied herein. Therefore, as reported previously for analogous degradation studies of conventional architecture PSC (FTO/compact-TiO_2/mesoporous-TiO_2/$MAPbI_3$/spiro-OMeTAD/Au), the device degradation observed in Figure 1c can be assigned to light and oxygen stress, with the AVA additive resulting in a 40-fold increase in device lifetime under 1 Sun illumination in ambient air.

In order to address the origin of this enhanced stability with AVA, we first investigated whether the enhanced stability in the presence of AVA is associated with the $MAPbI_3$ / TiO_2 interface. It has previously been suggested that the AVA, which contains both amine group and carboxyl acid groups, can function as a crosslinking agent between mesoporous TiO_2 and $MAPbI_3$.[23] To address this possibility, compact $MAPbI_3$ and AVA-$MAPbI_3$ thin films were directly deposited on glass slides without any mesoporous TiO_2 layer and then aged with the same air / light environmental stress as employed for the c-PSC devices in Figure 1c. Film degradation was tracked optically by detecting the RGB photobleaching of the perovskite films with a CCD camera (See ESI for details).[13] We expected that if the enhancement was due to the crosslinking effect of AVA, both AVA-$MAPbI_3$ and $MAPbI_3$ films should display similar stability in the absence of mesoporous TiO_2. However, as shown in Figure 2a, the $MAPbI_3$ thin film showed 50% photobleaching in 8 hours, while the AVA-$MAPbI_3$ took more than 108 hours to display a similar equal level of photobleaching. This enhancement of thin film stability in the absence of TiO_2, which is of similar magnitude to the increase in device stability, clearly indicates that AVA increases the stability of $MAPbI_3$ independently of any cross-linking effects with TiO_2.

We turn now to elucidating the origin of the enhanced stability of AVA-$MAPbI_3$ thin films relative to $MAPbI_3$ under light and oxygen stress. SEM images of the $MAPbI_3$ and AVA-$MAPbI_3$ thin films are shown in Figure 2b and 2c. It is apparent that the $MAPbI_3$ film has larger grain sizes than the AVA-$MAPbI_3$ film. It has previously been reported that perovskite decomposition initiates at grain boundaries and surfaces, typically with smaller grain sizes accelerating device degradation.[9,24] In contrary, improved stability in AVA-MAPbI3 is observed despite its smaller grain size. Thus, it can be concluded that this enhancement in stability does not originate from grain size differences.

As oxygen/light induced degradation has been shown to be initiated from perovskite grain boundaries and surface,[9] we suggest AVA is located at the termination of perovskite lattice. Herein, low-energy ion scattering (LEIS) spectroscopy was used to detect the surface first atomic layer of the film (Figure 3a). Firstly, the energy range between 0-1600 eV tells us about the presence of H on the surface; the higher decaying signal indicates that AVA-$MAPbI_3$ thin film has a higher concentration of H atoms on its surface. Secondly, since the yield has been dose corrected and the measurement was conducted below the static limit, the normalised data indicate lower concentrations of Pb and I atoms detected for AVA-$MAPbI_3$ compared to $MAPbI_3$. This is indicative of the presence of AVA molecules on AVA-$MAPbI_3$ film surface, as illustrated in Figure 3b. As herein the AVA cations are directly mixed into the $MAPbI_3$ precursor solution, rather than deposited as additional AVA cation layer on a preformed $MAPbI_3$ film, it appears very likely that AVA molecules will also be present at grain boundaries, terminating $MAPbI_3$ crystallites. Such terminations on crystallites may function as physical barriers to protect MAPbI3 from oxygen induced degradation.

Sun et al. have previously observed that perovskite films with higher defect densities are degraded faster under oxygen and light stress.[9] Oxygen/light degradation has also been suggested to be postponed by passivating surface defects using iodide salts or fullerene derivatives.[11,24] As such, we now turn to considering whether the enhanced stability of AVA-$MAPbI_3$ films observed herein may be associated with passivation of surface defects by AVA. Photoluminescence (PL) has been shown to be a sensitive probe of defect densities in $MAPbI_3$ films.[25] In Figure 3c, UV-Vis of these films did not show an obvious shift, indicating AVA-$MAPbI_3$ films have the same absorption and optical band gap as $MAPbI_3$ films. However, these films do show significant differences in steady-state photoluminescence (Figure 3d). Firstly, the AVA-$MAPbI_3$ films exhibit three times higher PL intensity than the $MAPbI_3$ films, indicating AVA passivates defect states in the perovskite which would lead to non-radiative recombination. Secondly, the PL peak position is shifted from 770 nm ($MAPbI_3$) to 763 nm (AVA-$MAPbI_3$). It has been previously reported that the $MAPbI_3$ PL peak can blue shift when trap/defect states are passivated.[26] Therefore, we can conclude that AVA is able to passivate trap / defect states in $MAPbI_3$ films, consistent with previous studies correlating lower defect densities and enhanced stability against oxygen/light induced degradation.[9]

We note that despite this trap state passivation, AVA-$MAPbI_3$ devices exhibited slightly lower device efficiencies. This most likely results from differences in the procedure for perovskite deposition (one-step rather than two-step, see ESI in details), which are likely to result in less complete infiltration of the precursor solution and/or crystallinity of the resulting perovskite light absorber.

In addition to the correlation between defect density and stability against light/oxygen induced degradation reported herein and previously, it has also been reported that oxygen can itself fill defects in $MAPbI_3$, resulting in increased PL emission.[27,28] As such, the impact of oxygen on film photoluminescence can have several different effects: it can act as an acceptor for $MAPbI_3$ electrons, resulting in a reduction in PL intensity; it can insert into surface $MAPbI_3$ defects, reducing the effect of electron trapping and thus increasing PL intensity; finally it can, in the presence of light, result in photodegradation of $MAPbI_3$, decreasing PL intensity. In order to unravel these complex interactions between oxygen and $MAPbI_3$ and their impact upon PL intensity, we monitored the PL of $MAPbI_3$ and AVA-$MAPbI_3$ films as a function of time after oxygen exposure (Figures 4a-c). Samples were initially stored in N_2 filled quartz cuvettes, and 20 vol% oxygen introduced into the cuvette after the first PL scan. We observed that the PL intensity of $MAPbI_3$ films increased over time following oxygen exposure (Figure 4a), consistent with previous reports.[27,28] This increase is attributed, as previously, to oxygen binding to surface defects, partially passivating these defects and reducing their tendency to function as electron traps (Pathway 1 in the insert to Figure 4c). This increase in PL intensity saturated after 1000 seconds, after this it started to decrease, alongside the appearance of a low energy tail of the PL spectrum (Figure S2). Such a low energy tail of the PL is also observed in $MAPbI_3$ film with excess PbI_2 or MAI in the literature, and is indicative of superoxide induced degradation of $MAPbI_3$.[29,30] As such, this decrease at long times is assigned to $MAPbI_3$ degradation, with the timescale being consistent with the photobleaching data shown in Figure 2 above. In contrast, AVA-$MAPbI_3$ films showed a pronounced decrease of PL intensity when exposed to oxygen in Figure 4b (although from a much higher initial value). The timescale for this decrease in PL intensity (decays half-time of ~150 s) is similar to timescales previously reported for oxygen to diffuse into $MAPbI_3$ grain boundaries.[24] This PL quenching cannot attributed to perovskite degradation as AVA-$MAPbI_3$ has shown to be stable on this time scale in Figure 2a. Rather this quenching of PL in the presence of oxygen can be attributed to electron transfer from AVA-$MAPbI_3$ grains to oxygen molecules in grain boundaries (pathway 2 in Figure 4c), resulting in superoxide formation. This observation is consistent with surface defect states already being occupied by AVA in this film, such that oxygen binding into such states is inhibited.

To sum up, we suggest there are two pathways leading to the PL intensity changes on the 100-1000s timescale in the films studied herein. This timescale corresponds to the timescale of oxygen diffusion into film grain boundaries, but it is faster than the timescale of light and oxygen induced photodegradation. Oxygen binding into perovskite surface defects can result in PL intensity increasing (Pathway 1 in Figure 4c), while oxygen in grain boundaries which does not incorporate into perovskite defects can reduce PL intensity (Pathway 2 in Figure 4c). Because the $MAPbI_3$ film is rich in unpassivated surface defects, Pathway 1 dominates over Pathway 2, leading to the enhanced PL intensity. However such oxygen binding into surface defects does not protect the film against light and oxygen induced degradation, consistent with the reduction in PL intensity observed at long times, correlated with the photobleaching data in Figure 2. In contrast, as AVA has already effectively passivated these defects in AVA-$MAPbI_3$, oxygen is unable to incorporate into these defects and pathway 1 is inactive. Therefore, the Pathway 2 dominates in AVA-$MAPbI_3$ films, resulting in the observed reduction in PL intensity. These counterpoised effects of oxygen on the PL intensity of $MAPbI_3$ and AVA-$MAPbI_3$ films clearly illustrate the differing effects of oxygen on the film photophysics, as discussed further below.

Previously, we have proposed that the oxygen/light degradation is mediated by superoxide, which is generated when the oxygen accepts a photoexcited electron from $MAPbI_3$.[24] To evaluate the formation of superoxide (O_2^-) in $MAPbI_3$ and AVA-$MAPbI_3$ films, we monitored the superoxide formation by the hydroethidine (HE) molecular fluorescent probe, which exhibits a characteristic increase in fluorescence following O_2^- exposure, as previously reported.[10] As plotted in Figure 4d, it is apparent that an AVA-$MAPbI_3$ film shows higher generation of free superoxide than a $MAPbI_3$ film. As AVA-$MAPbI_3$ demonstrates superior thin film stability to $MAPbI_3$, we can conclude that this enhanced stability derives not from suppression of superoxide generation but rather from higher resistance to superoxide induced degradation. We note that we have previously reported an analogous result in a comparison of the stability of $MAPbI_3$ and $MAPbBr_3$ films, where we observed efficiently generated superoxide but resistance to superoxide mediated degradation, attributed in this case to the superior chemical stability of $MAPbBr_3$.[13] Our observation that AVA-$MAPbI_3$ films generate more superoxide than $MAPbI_3$ can most likely be attributed to their higher density of grain boundaries (due to their small grain sizes), facilitating oxygen diffusion in, and superoxide diffusion out, of these films.

Based upon these results and previous literature, we summarise by proposing a simple model to explain the enhanced stability of AVA-$MAPbI_3$ to light and oxygen induced degradation, as illustrated in Figure 5. In the absence of AVA, oxygen can bind to surface defect sites on $MAPbI_3$ crystallites (Process 'A' in Figure 5). This results in a modest enhancement of PL intensity due to partial surface defect state passivation. AVA can also bind to such surface defects, resulting in a much more effective defect site passivation, and preventing subsequent oxygen binding to these sites. Photoexcitation of both $MAPbI_3$ and AVA-$MAPbI_3$ in the presence of oxygen can result in the reduction of oxygen in grain boundaries, resulting in free superoxide generation, as observed in our superoxide probe measurements (Figure 4d). However, as suggested previously, degradation of perovskite by superoxide requires access to surface defects.[24] The passivation of surface defects by AVA prevents superoxide mediated degradation and greatly enhances stability. In the absence of AVA, superoxide is able to access surface defects and induce degradation (Process 'B' in Figure 5). It is also possible this degradation may result from the reduction of oxygen already bound in defect sites (Process 'A'), although our data cannot separately observe this. Overall these results indicate that the enhanced stability of AVA-$MAPbI_3$ films results from the passivation of surface defect sites which otherwise can mediate superoxide induced degradation.

In conclusion, we demonstrate that using AVA-$MAPbI_3$ as an active layer in c-PSC structure device results in ~40 times longer operational lifetime than $MAPbI_3$ in ambient air (RH ~15%). This improvement is also observed in thin film stability, revealing it is correlated to perovskite itself rather than the interaction between perovskite and any other interlayers. Consequently, it may be possible to apply this passivation technique to stabilise other device architectures.

AVA is found to be located at the grain surface of $MAPbI_3$, passivating surface defects. The AVA-$MAPbI_3$ with lower defects density demonstrate higher resistance to oxygen and light stress than $MAPbI_3$. Even though AVA-$MAPbI_3$ film generates more superoxide than $MAPbI_3$ film, AVA-$MAPbI_3$ demonstrates higher superoxide resistivity. The passivation of surface defects by AVA results in physical barrier to protect $MAPbI_3$ from superoxide induced degradation in grain boundary, prolonging the lifetime of both thin films and devices under oxygen/light stress. Therefore, in this study we deduce the origin of improved stability of AVA-$MAPbI_3$ c-PSC device and highlight the strategy of passivation of perovskite's grain termination to enhance its resistance to oxygen/light degradation.

Conflicts of interest

There are no conflicts to declare.

Acknowledgment

We thank Welsh government funded Sêr Solar project, as well as the EPSRC Plastic Electronics CDT, the UKRI Global Challenge Research Fund project SUNRISE (EP/P032591/1), Self - assembly Perovskite Absorber layers - Cells Engineered into Modules Project (EP/M01524/2), SPECIFIC IKC (EP/N02083/1) and the CSC for financial support, as well as Xiaoe Li for technical support.

Reference

1 W. S.Yang, B.-W.Park, E. H.Jung, N. J.Jeon, Y. C.Kim, D. U.Lee, S. S.Shin, J.Seo, E. K.Kim, J. H.Noh andS.IlSeok, *Science (80-.).*, 2017, **356**, 1376–1379.

2 K.Yoshikawa, H.Kawasaki, W.Yoshida, T.Irie, K.Konishi, K.Nakano, T.Uto, D.Adachi, M.Kanematsu, H.Uzu andK.Yamamoto, *Nat. Energy*, 2017, **2**, 17032.

3 J. H.Noh, S. H.Im, J. H.Heo, T. N.Mandal andS.IlSeok, *Nano Lett.*, 2013, **13**, 1764–1769.

4 Z.Song, C. L.McElvany, A. B.Phillips, I.Celik, P. W.Krantz, S. C.Watthage, G. K.Liyanage, D.Apul andM. J.Heben, *Energy Environ. Sci.*, 2017, **10**, 1297–1305.

5 J.-H.Im, C.-R.Lee, J.-W.Lee, S.-W.Park andN.-G.Park, *Nanoscale*, 2011, **3**, 4088.

6 R. E.Brandt, V.Stevanovi??, D. S.Ginley andT.Buonassisi, *MRS Commun.*, 2015, **5**, 265–275.

7 D.Bryant, N.Aristidou, S.Pont, I.Sanchez-Molina, T.Chotchunangatchaval, S.Wheeler, J. R.Durrant andS. A.Haque, *Energy Environ. Sci.*, 2016, **9**, 1655–1660.

8 A. M. A.Leguy, Y.Hu, M.Campoy-Quiles, M. I.Alonso, O. J.Weber, P.Azarhoosh, M.VanSchilfgaarde, M. T.Weller, T.Bein, J.Nelson, P.Docampo andP. R. F.Barnes, *Chem. Mater.*, 2015, **27**, 3397–3407.

9 Q.Sun, P.Fassl, D.Becker-Koch, A.Bausch, B.Rivkin, S.Bai, P. E.Hopkinson, H. J.Snaith andY.Vaynzof, *Adv. Energy Mater.*, 2017, **1700977**, 20.

10 N.Aristidou, I.Sanchez-Molina, T.Chotchuangchutchaval, M.Brown, L.Martinez, T.Rath andS. aHaque, *Angew. Chem. Int. Ed. Engl.*, 2015, **54**, 1–6.

11 C.-T.Lin, S.Pont, J.Kim, T.Du, S.Xu, X.Li, D.Bryant, M. A.Mclachlan andJ. R.Durrant, *Sustain. Energy Fuels*, 2018, **2**, 1686–1692.

12 M.Saliba, T.Matsui, J.-Y.Seo, K.Domanski, J.-P.Correa-Baena, M. K.Nazeeruddin, S. M.Zakeeruddin, W.Tress, A.Abate, A.Hagfeldt andM.Grätzel, *Energy Environ. Sci.*, 2016, **9**, 1989–1997.

13 S.Pont, D.Bryant, C.-T.Lin, N.Aristidou, S.Wheeler, X.Ma, R.Godin, S. A.Haque andJ. R.Durrant, *J. Mater. Chem. A*, 2017, **5**, 9553–9560.

14 A.Mei, X.Li, L.Liu, Z.Ku, T.Liu, Y.Rong, M.Xu, M.Hu, J.Chen, Y.Yang, M.Grätzel andH.Han, *Science (80-.).*, 2014, **345**, 295–298.

15 M.Hu, L.Liu, A.Mei, Y.Yang, T.Liu andH.Han, *J. Mater. Chem. A Mater. energy Sustain.*, 2014, **2**, 17115–17121.

16 Y.Hu, S.Si, A.Mei, Y.Rong, H.Liu, X.Li andH.Han, *Sol. RRL*, 2017, **1**, 1600019.

17 G.Grancini, C.Roldán-Carmona, I.Zimmermann, E.Mosconi, X.Lee, D.Martineau, S.Narbey, F.Oswald, F.DeAngelis, M.Graetzel andM. K.Nazeeruddin, *Nat. Commun.*, 2017, **8**, 15684.

18 H.Tsai, W.Nie, J.-C.Blancon, C. C.Stoumpos, R.Asadpour, B.Harutyunyan, A. J.Neukirch, R.Verduzco, J. J.Crochet, S.Tretiak, L.Pedesseau, J.Even, M. A.Alam, G.Gupta, J.Lou, P. M.Ajayan, M. J.Bedzyk, M. G.Kanatzidis andA. D.Mohite, *Nature*, 2016, **536**, 312–316.

19 X.Li, M.Ibrahim Dar, C.Yi, J.Luo, M.Tschumi, S. M.Zakeeruddin, M. K.Nazeeruddin, H.Han andM.Grätzel, *Nat. Chem.*, 2015, **7**, 703–711.

20 C.Chan, Y.Wang, G.Wu andE. W.Diau, *J. Mater. Chem. A Mater. energy Sustain.*, 2016, **4**, 3872–3878.

21 J.Baker, K.Hooper, S.Meroni, A.Pockett, J.McGettrick, Z.Wei, R.Escalante, G.Oskam, M.Carnie andT.Watson, *J. Mater. Chem. A*, 2017, **5**, 18643–18650.

22 K.Domanski, E. A.Alharbi, A.Hagfeldt, M.Grätzel andW.Tress, *Nat. Energy*, 2018, **3**, 61–67.

23 Y. C.Shih, Y. B.Lan, C. S.Li, H. C.Hsieh, L.Wang, C. I.Wu andK. F.Lin, *Small*, 2017, **13**, 1–10.
24 N.Aristidou, C.Eames, I.Sanchez-Molina, X.Bu, J.Kosco, M. S.Islam andS. A.Haque, *Nat. Commun.*, 2017, **8**, 15218.
25 N. K.Noel, A.Abate, S. D.Stranks, E. S.Parrott, V. M.Burlakov, A.Goriely andH. J.Snaith, *ACS Nano*, 2014, **8**, 9815–9821.
26 Y.Shao, Z.Xiao, C.Bi, Y.Yuan andJ.Huang, *Nat. Commun.*, 2014, **5**, 1–7.
27 R.Brenes, D.Guo, A.Osherov, N. K.Noel, C.Eames, E. M.Hutter, S. K.Pathak, F.Niroui, R. H.Friend, M. S.Islam, H. J.Snaith, V.Bulović, T. J.Savenije andS. D.Stranks, *Joule*, 2017, **1**, 155–167.
28 Y.Tian, M.Peter, E.Unger, M.Abdellah, K.Zheng, T.Pullerits, A.Yartsev, V.Sundström andI. G.Scheblykin, *Phys. Chem. Chem. Phys.*, 2015, **17**, 24978–24987.
29 T.Du, J.Kim, J.Ngiam, S.Xu, P. R. F.Barnes, J. R.Durrant andM. A.McLachlan, *Adv. Funct. Mater.*, 2018, 1801808.
30 V.Kapoor, A.Bashir, L. J.Haur, A.Bruno, S.Shukla, A.Priyadarshi, N.Mathews andS.Mhaisalkar, *Energy Technol.*, 2017, **5**, 1880–1886.

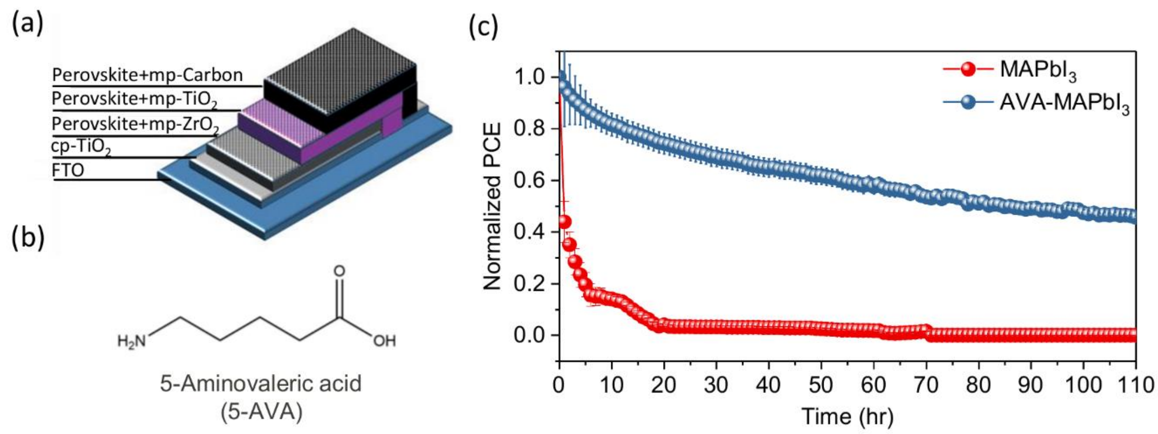

Figure 1. (a) Device configuration of multi-layer screen printed mesoporous stack perovskite solar cell (c-PSC) consisted of FTO/compact-TiO_2/mesoporous-TiO_2/mesoporous-ZrO_2/mesoporous-carbon. (b) Chemical structure of 5-aminovaleric acid. (c) Normalized device stability of $MAPbI_3$ and AVA-$MAPbI_3$ devices. Stability were measured under ambient air (RH ~15%) and continuous illumination provided by LED. Light intensity of LED was calibrated to provide equivalent Jsc measured under AM 1.5 solar simulator with 1 sun intensity.

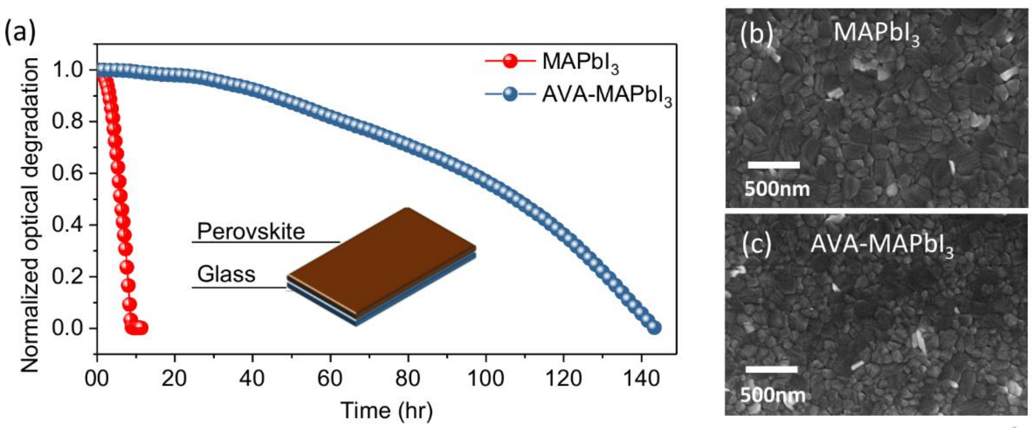

Figure 2. (a) Normalized optical degradation of $MAPbI_3$ and AVA-$MAPbI_3$ thin film on glass in ambient air (RH ~15%) with full sun illumination provided by LED array. SEM images of (b) $MAPbI_3$ and (c) AVA-$MAPbI_3$.

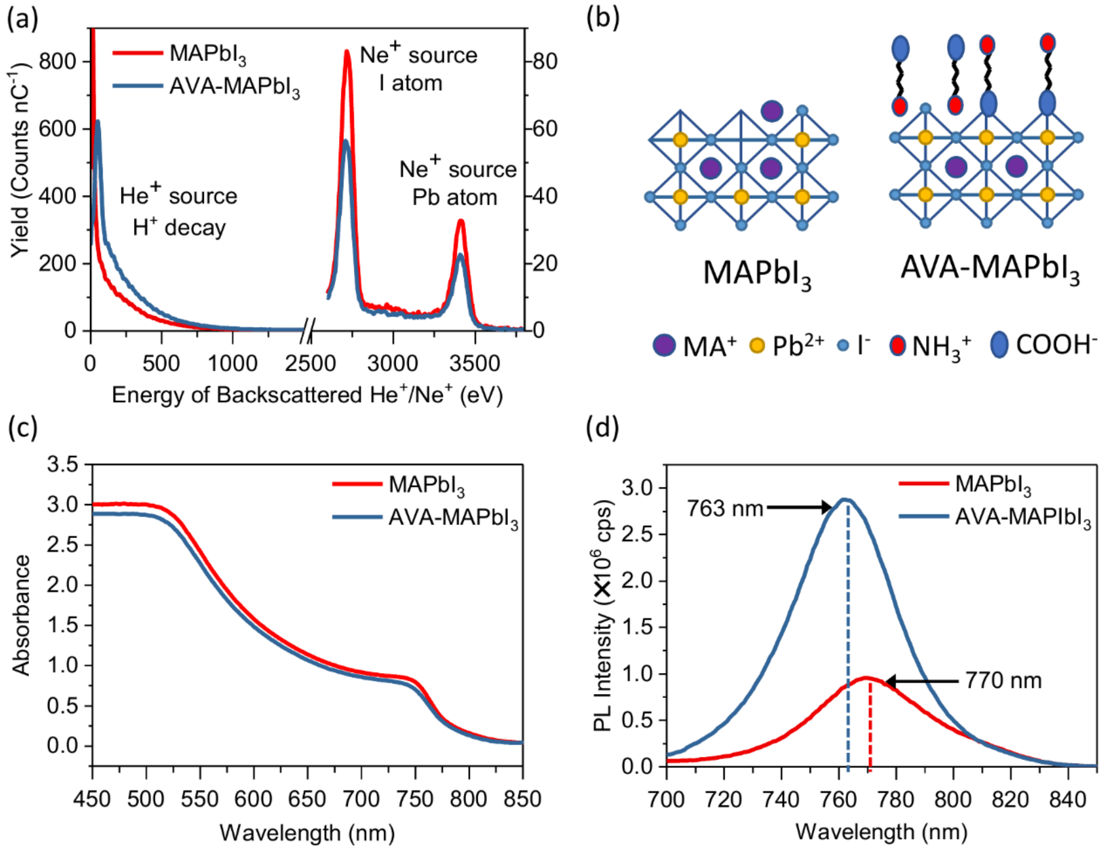

Figure 3. (a) Low-energy ion scattering (LEIS) measurement of $MAPbI_3$ and AVA-$MAPbI_3$ films. Ne^+ plasma was used to detect Pb and I atoms. He^+ plasma was used to detect H^+ decay. (b) Schematic representation of AVA passivation at lattice termination of $MAPbI_3$ (c) UV-visible and (d) steady-state photoluminescence (PL) spectra of $MAPbI_3$ and AVA-$MAPbI_3$ films. PL spectra were measured under full sun illumination provided by LED array with 700 nm low pass filter.

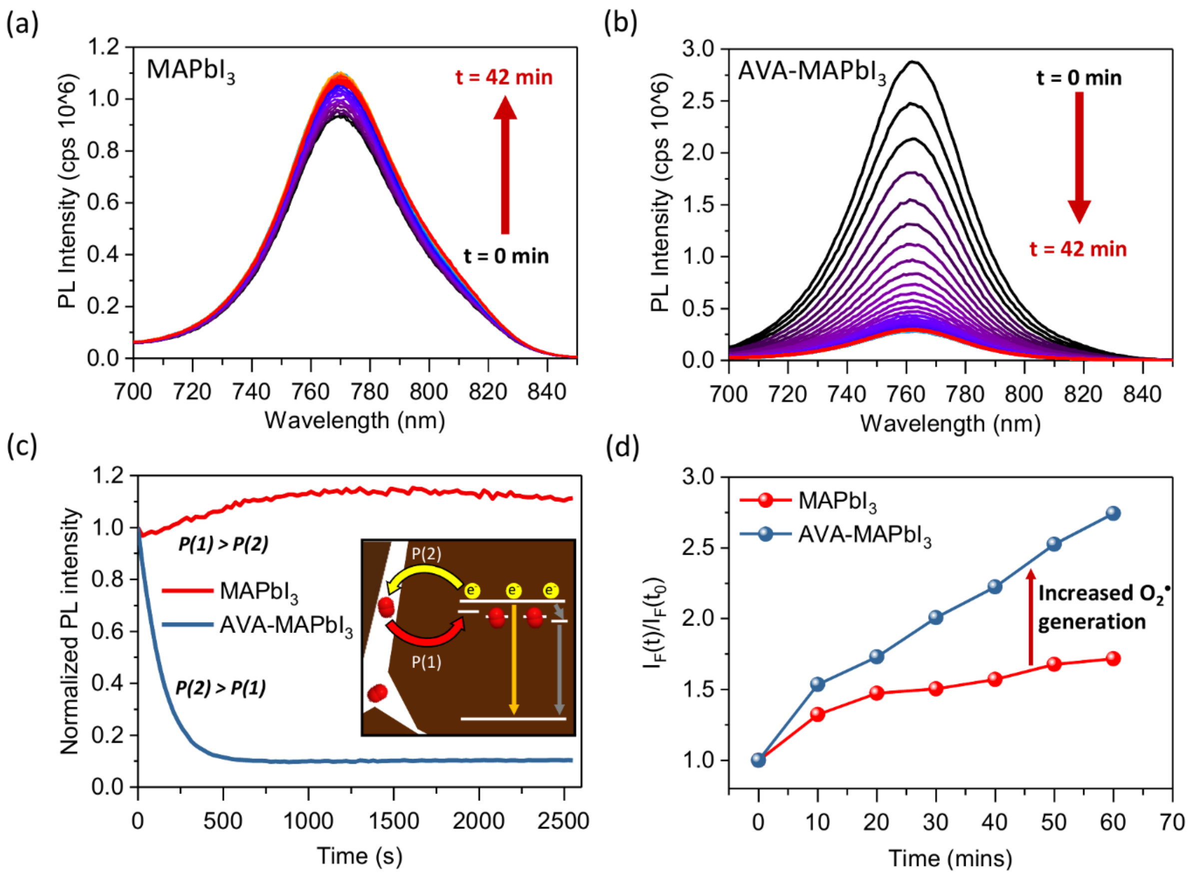

Figure 4. PL spectra of (a) $MAPbI_3$ and (b) AVA-$MAPbI_3$ as a function of time after exposure to oxygen (employing LED excitation as for Figure 3). (c) PL peak intensity versus time following exposure to oxygen, taken from the data in (a) and (b). Inserted illustration diagram provides two possible pathway of PL changes. Pathway1 is the oxygen incorporated into perovskite defects leading to increased PL intensity. Pathway2 is the oxygen at grain boundaries quenching the PL intensity. (d) Fluorescence intensity of a molecular probe for superoxide as a function of perovskite film irradiation time in the presence of oxygen. Fluorescence intensity probed at 610 nm with excitation at 520 nm, where IF(t) is the fluorescence intensity at time t, and IF(t_0) is at 0 minutes. The IF(t)/ IF(t_0) ratio is measure of the amount of superoxide generated by irradiation of the perovskite films.

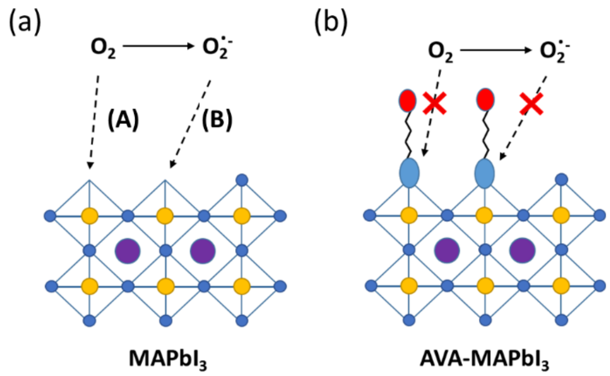

Figure 5. Schematic representation of enhanced stability resulting from AVA passivation of surface defect sites of $MAPbI_3$. In the absence of AVA (a), oxygen can access iodide vacancies at grain boundaries, resulting under irradiation in superoxide mediated photodegradation. In the presence of AVA (b), AVA binds to these iodide vacancies, inhibiting this degradation.